Global Minimization of the Active Contour Model with TV-Inpainting and Two-phase Denoising

Shingyu Leung and Stanley Osher
Department of Mathematics, UCLA
Los Angeles, CA 90095
{syleung,sjo}@math.ucla.edu

Abstract

The active contour model [9, 10, 2] is one of the most well-known variational methods in image segmentation. In a recent paper by Bresson, Esedoḡlu, Vandergheynst, Thiran and Osher [1], a link between the active contour model and the variational denoising model of Rudin-Osher-Fatemi (ROF) [12] was demonstrated. This relation provides a method to determine the **global** *minimizer of the active contour model. In this paper, we propose a variation of this method to determine the global minimizer of the active contour model in the case when there are missing regions in the observed image. The idea is to turn off the L^1-fidelity term in some subdomains, in particular the regions for image inpainting. Minimizing this proposed energy provides a unified way to perform image denoising, image segmentation and image inpainting. To determine the minimizer of this energy functional, we use the method of gradient descent. But unlike the usual numerical method which uses the standard fully explicit scheme, we apply the Alternating Direction Explicit (ADE) scheme. This scheme provides a faster and a more robust way to minimize the proposed energy functional.*

1 Introduction

Image segmentation, image restoration and image inpainting are a few basic yet important areas in image processing and computer vision. Traditionally, these closely related fields were developed independently. However, the use of the level set method and variational methods in recent years started to bring all these fields together. One example is the TV-inpainting model [7]. We can perform inpainting in a desired domain while applying the ROF model [12] to remove noise from the rest of the domain using only one energy functional. Another example is the Mumford-Shah model [11] which was originally designed for image segmentation but can also be used as an image denoising tool. Extension of the Mumford-Shah model to image inpainting was also carried out in [8].

There are two interesting recent developments about the connection between different fields in image processing. We will discuss later in this paper how they link different fields in an interesting way. The first development concerns the impulse-noise removal method and the variational method for image regularization. In two recent papers by Chan, Nikolova et al. [3, 4], a two-phase method was proposed to remove impulse-type noise. For a true image $u^*(x)$ and an observed image $f(x)$ defined in a domain Ω, impulse-type noise is defined by

$$f(x) = \begin{cases} r(x) & \text{with probability } r_0 \\ u^*(x) & \text{with probability } (1-r_0). \end{cases} \tag{1}$$

As an example, for the so-called salt-and-pepper noise, $r(x)$ is simply the maximum or the minimum of the image intensity (0 and 255 for grey-scaled images). The main idea in those papers is to separate the denoising process into a noise detection phase and a noise removal phase. In the first stage, a median-type filter is applied to the observed image to detect the possible locations of the impulse noise. Then in the second phase, instead of replacing the intensity at all locations by the median intensity around a certain neighborhood, a L^1-regularization method is applied only to those locations reported in the first phase while keeping the other pixels unchanged. The resulting method was shown to be able to remove the salt-and-pepper noise efficiently even at a very high noise level (for example $r_0 = 0.75$). The main reason for its success is that this method retains those pixels that are unlikely to be polluted and maintains sharp edges in the whole image.

Another interesting development is a new model that uses variational method for image segmentation [5, 1]. The idea of the model is to minimize an energy functional consisting of a weighted TV-norm with a L^1-fidelity term. For the segmentation of a binary image, the papers showed an equivalence between the new energy functional and that of the active contour model. This relation can be used to overcome the problem of the active contour model in which the energy function is not convex. Very often the snake will be trapped in a **local** minimizer thus giving unsatisfactory segmentation results. The link between these two energies, as demonstrated in the above papers, provides a convenient way to determine the **global** minimizer of the active contour energy.

In this paper, we will combine the two recent advances in image processing mentioned above. This provides an efficient and unified way to perform image denoising (for both impulse-type and Gaussian-type noises), image segmentation, and image inpainting at the same time.

The rest of the paper will be organized as follows. In Section 2, we will briefly review the denoising model by Chan, Nikolova et al. [3, 4] and also restate the link between the active contour model and the ROF model as in [1]. A new model will be given in Section 3. Section 4 contains some details in the numerical implementation. Some numerical results will be given in Section 5.

2 Two Recent Developments

2.1 A Two-Phase Method to Remove Impulse-type Noise

Unlike the usual way to denoise impulse noise by applying the median-type filter to the image and replacing the image intensity everywhere, the idea in [3, 4] is to separate the denoising processing into a noise-detection phase and a noise-removal phase. Mathematically, the first phase can be formulated as determining a noise candidate set

$$\mathcal{N} = \{x \in \Omega : f(x) \neq f_{\text{MF}}(x)\} \tag{2}$$

in which Ω is the image domain, $f(x)$ is the observed image intensity at the pixel x, and $f_{\text{MF}}(x)$ is the intensity at x after applying a median-type filter, such as the classical median filter or the adaptive median filter. In the second phase, the following functional is minimized

$$F|_{\mathcal{N}}(u) = \int_{\mathcal{N}} \left\{ |u(x) - f(x)| + \frac{\beta}{2}[S_1(u) + S_2(u)] \right\} \tag{3}$$

where

$$\begin{aligned} S_1(u) &= \int_{\mathcal{V}(x)\cap(\Omega\setminus\mathcal{N})} 2\,\phi[u(x) - f(y)]dy \\ S_2(u) &= \int_{\mathcal{V}(x)\cap\mathcal{N}} \phi[u(x) - u(y)]dy\,, \end{aligned} \tag{4}$$

$\mathcal{V}(x)$ is the neighborhood centered at x and ϕ is an edge-preserving potential function. As seen in [3, 4], one possible choice for ϕ is

$$\phi(t) = \sqrt{t^2 + \epsilon^2} \tag{5}$$

with a small constant ϵ. The first term in the curve-bracket is a L^1-fidelity term. The terms in the square-bracket can be interpreted as an approximation of the total variation (TV) of u.

In the simple case when the noise can be separated accurately in the first step, the fidelity term is not important. A simplification of this whole algorithm is therefore the same as an image inpainting algorithm. For example, if ROF [12] or L^2-fidelity is used instead, we arrive at the TV-inpainting [7]. That is, given an observed image f, one minimizes the following energy

$$E_1(u) = \int_\Omega |\nabla u| + \frac{1}{2}\int_\Omega \lambda(x)|u - f|^2 \tag{6}$$

where

$$\lambda(x) = \begin{cases} 0 & \text{if } f(x) = f_{\text{MF}}(x) \\ \lambda_\infty \simeq \infty & \text{otherwise.} \end{cases} \tag{7}$$

The idea of using a piecewise constant $\lambda(x)$ in TV-inpainting is not new [7]. However, it is interesting to see here the relationship between the impulse-type noise removal and image inpainting by using a piecewise constant $\lambda(x)$ determined by a median-type filter.

2.2 Global Minimizer of the Active Contour Model

In the classical active contour model, the initial guess of the segmented image plays a very important role. We show in Figure 1 some minimizers of the active contour model. As we can see, different initial conditions in the evolution will give different segmented region. More importantly, none of these results corresponds to the *true* segmented results, i.e. curves which separate all regions with different intensities in the whole image. One reason for these unsatisfactory results is that the minimization problem of the active contour is not convex, and therefore it is very likely that the energy minimization could be trapped into a **local** minimizer, as shown in the left most case.

Recently, a few algorithms were proposed [5, 1] to determine the **global** minimizers of some image segmentation models. In particular, an algorithm to determine the global minimizer of the active contour model based on the ROF model was given in [1]. The idea is to modify the ROF energy

$$E_{\text{ROF}}(u, \lambda) = \int_\Omega |\nabla u| + \frac{\lambda}{2}\int_\Omega |u - f|^2 \tag{8}$$

by first replacing the TV-norm by a weighted TV-norm and then, more importantly, changing the measure in the fidelity

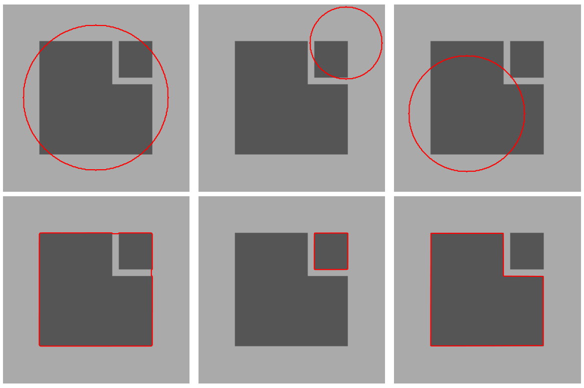

Figure 1. Segmentation results using the active contour model. We show different initial configurations of the snake on the first row. The corresponding segmented results using these initial conditions are shown on the second row.

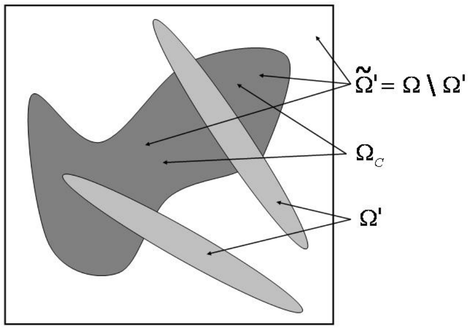

Figure 2. Problem setting. Definition of the set Ω' (domain for inpainting), $\tilde{\Omega}'$ (compliment of Ω') and Ω_C (domain bounded by the curve C).

term from L^2-norm to L^1-norm. This gives

$$E_2(u,\lambda) = \int_\Omega \tilde{g}(f)|\nabla u| + \lambda \int_\Omega |u - f| \tag{9}$$

in which

$$\tilde{g}(f) = \frac{1}{1+\beta|\nabla f|^2}\,. \tag{10}$$

As pointed out in [1], if u is the characteristic function of a set Ω_C with boundary given by the curve C (i.e. $u = \mathbf{1}_{\Omega_C}$), the minimizer of the above energy E_2 is the same as the minimizer of the active contour energy

$$E_{\text{AC}}(C) = \int_C \tilde{g}(f)ds \tag{11}$$

with f approximated (in the sense of L^1) by a binary function of a region Ω_C.

Numerically, the minimization problem (9) is convex. This means that the method of gradient descent will converge to a unique minimizer, i.e. the global minimum of the energy function, independent of the initial condition. The significance of this equivalence is that by minimizing (9), one can determine the global minimizer of the active contour model (11) without the danger of trapping into any local minimum and the uncertainty in picking an initial configuration of the snake.

3 The New Energy

3.1 The Energy

Here, we propose a new model to combine the two recent developments in image processing. Given an observed image f, we minimize the energy

$$E(u) = \int_\Omega g(f)|\nabla u| + \int_\Omega \lambda(x)|u-f|\,. \tag{12}$$

This energy is similar to (9), except that $\lambda(x)$ is now changed to a function in space and the weight in the weighted TV-norm is also modified. The function $\lambda(x)$ has the following properties.

$$\lambda(x) = \begin{cases} 0 & \text{TV-inpainting} \\ \lambda_0 & \text{Denoising} \\ \lambda_\infty \simeq \infty & \text{Unchanged.} \end{cases} \tag{13}$$

In the subdomain for image inpainting, $f(x)$ (and therefore $\tilde{g}(f)$) might not be known. We therefore set $g(f) = 1$, or $\beta = 0$. For the rest of the domain, we keep $g(f) = \tilde{g}(f)$. In other words, we have

$$g(f) = \begin{cases} 1 & \text{if } \lambda(x) = 0 \\ \tilde{g}(f) \equiv (1+\beta|\nabla f|^2)^{-1} & \text{otherwise.} \end{cases} \tag{14}$$

Mathematically, minimizing the above energy (12) is the same as

$$\min_u \int_\Omega g(f)|\nabla u| \tag{15}$$

such that

$$\int_\Omega \omega(x)|u-f| = \text{ constant} \tag{16}$$

for some weighted function $\omega(x)$. Therefore, the way to determine $\lambda(x)$ is equivalent to the way to spread the error in approximating the observed image f.

Here we give some suggestions in picking such $\lambda(x)$ and also provide a variation in using the above minimization algorithm.

For the salt-and-pepper noise, the following $\lambda(x)$ works efficiently. We define $d(x)$ to be the difference in the intensities between the original image $f(x)$ and the modified image after applying the median-type filter $f_{\text{MF}}(x)$, i.e.

$$d(x) = |f(x) - f_{\text{MF}}(x)|\,. \tag{17}$$

Then one can set

$$\lambda_1(x) = \begin{cases} \lambda_\infty & \text{if } d(x) = 0 \text{ and } x \notin \Omega' \\ 0 & \text{otherwise} \end{cases} \tag{18}$$

where $\Omega' \subset \Omega$ is a given subdomain for doing image inpainting and is characterized by an user predefined mask function. This means that if x is in the inpainting domain Ω' or if the noise-detector detects that the image at x is polluted (therefore $f(x)$ will be different from the intensity after applying the median-type filter $f_{\text{MF}}(x)$), then the intensity at x will be modified by a TV-type regularization. Otherwise, the intensity at that location will remain unchanged.

If the impulse noise is random-valued instead, one can use a similar $\lambda(x)$

$$\lambda_2(x) = \begin{cases} \lambda_0 & \text{if } d(x) = 0 \text{ and } x \notin \Omega' \\ 0 & \text{otherwise} \end{cases} \tag{19}$$

with $\lambda_0 << \lambda_\infty$.

For the Gaussian-type noise, one can simply use

$$\lambda_3(x) = \begin{cases} \lambda_0 & \text{if } x \notin \Omega' \\ 0 & \text{otherwise.} \end{cases} \tag{20}$$

In the case when the type of noise is not known *a priori*, one can try to minimize (12) iteratively. More specifically, given the observed image $u_0 = f$, for $m = 1, \cdots, m_{\max}$, one minimizes

$$E(u_m) = \int_\Omega g(u_{m-1})|\nabla u_m| + \int_\Omega \lambda_4(x)|u_m - u_{m-1}| \tag{21}$$

iteratively with

$$\lambda_4(x) = \begin{cases} \lambda_0 & \text{if } d(x) \le d^* \text{ and } x \notin \Omega' \\ 0 & \text{otherwise} \end{cases} \tag{22}$$

where d^* is a threshold in the intensity difference function $d(x) \equiv |u_{m-1} - (u_{m-1})_{\text{MF}}|$.

3.2 The Link Between Active Contour for Segmentation, Denoising and TV-Inpainting

The relations between the minimization of the energy functional (12), the active contour model and the TV-inpainting model are explained here.

Assuming $\Omega' = \{x \in \Omega : \lambda(x) = 0\}$ is the subdomain for inpainting (notice that $\mathcal{N} \subset \Omega'$) and $\tilde{\Omega}' = \Omega \setminus \Omega'$, we have

$$\begin{aligned} E(u) &= \int_{\tilde{\Omega}'} g(f)|\nabla u| + \int_{\tilde{\Omega}'} \lambda_0|u-f| + \int_{\Omega'} |\nabla u| \\ &= E^1(u) + E^2(u) \end{aligned} \tag{23}$$

where

$$\begin{aligned} E^1(v) &= \int_{\tilde{\Omega}'} g(f)|\nabla v| + \int_{\tilde{\Omega}'} \lambda_0|v-f| \\ E^2(w) &= \int_{\Omega'} |\nabla w| \end{aligned} \tag{24}$$

with $v : \tilde{\Omega}' \to [u_{\min}, u_{\max}]$ and $w : \Omega' \to [u_{\min}, u_{\max}]$. So minimizing $E(u)$ is the same as

$$\min_v E^1(v) + \min_w E^2(w)\,, \tag{25}$$

and the minimizer of $E(u)$ is given by $u = \mathbf{1}_{\tilde{\Omega}'}(x) \cdot v + \mathbf{1}_{\Omega'}(x) \cdot w$ in which $\mathbf{1}_{\tilde{\Omega}'}$ is the characteristic function of the set $\tilde{\Omega}'$.

First we consider the energy $E^1(v)$. If Ω_C is a set in $\tilde{\Omega}'$ whose boundary is denoted by C and if the minimizer of $E^1(v)$ is given by $v = \mathbf{1}_{\Omega_C}$, then we have

$$\begin{aligned} E^1(v) &= \int_{\tilde{\Omega}'} g(f)|\nabla \mathbf{1}_{\Omega_C}| + \int_{\tilde{\Omega}'} \lambda_0|\mathbf{1}_{\Omega_C} - f| \\ &= \int_C g(f)ds + \int_{\tilde{\Omega}'} \lambda_0|\mathbf{1}_{\Omega_C} - f|\,. \end{aligned} \tag{26}$$

Therefore, minimizing $E^1(v)$ in the subdomain $\tilde{\Omega}'$ in the case of a binary observed image is equivalent to minimizing the active contour energy in $\tilde{\Omega}'$, given by

$$\min_C \int_C g(f)ds \tag{27}$$

while

approximating f (in the L^1 sense) in $\tilde{\Omega}'$
by a binary function of the set/region Ω_C.

For the energy $E^2(w)$ defined in the complement, Ω', we have

$$E^2(w) = \int_{\Omega'} |\nabla w| \tag{28}$$

together with the boundary condition $w|_{\partial\Omega'} = v|_{\partial\Omega'}$ where v is the minimizer of $E^1(v)$. In the case when v is binary on $\partial\Omega'$, we have $w = \mathbf{1}_{\Omega_{C'}}$ again. This gives

$$E^2(w) = \int_{\Omega'} |\nabla \mathbf{1}_{\Omega_{C'}}| = \int_{C'} ds\,. \tag{29}$$

This implies that when the boundary $\partial\Omega'$ is binary valued, minimizing $E^2(w)$ in Ω' is equivalent to

$$\min_{C'} \int_{C'} ds \tag{30}$$

while the end points of C' are fixed on $\partial\Omega'$. Further analysis on the behavior of TV-inpainting can be found in [6].

4 Numerical Method

To minimize the above energy, one can use the method of gradient descent. The Euler-Lagrange equation of the energy functional (12) is given by

$$\frac{\partial u}{\partial t} = \nabla \cdot \left(\frac{g(x)}{|\nabla u|} \nabla u \right) - \lambda(x) \frac{u-f}{|u-f|} \,. \qquad (31)$$

Here we give the details of the algorithm in updating u^{n+1} by solving (31) using the Alternative Direction Explicit (ADE) technique. This numerical scheme is second order accurate in time for linear equations and fully explicit but yet unconditionally stable for any time-step Δt. Given the observed image f and an intermediate approximation u^n, we use the following procedures.

1. Define $v^n = u^n$ and $w^n = u^n$.

2. Compute

$$\begin{aligned} h_{i,j}^{x\pm} &= \{1+\beta[(D_x^{\pm} f_{i,j})^2 + (D_y^0 f_{i,j})^2]\}^{-1} \\ &\quad [(D_x^{\pm} u_{i,j}^n)^2 + (D_y^0 u_{i,j}^n)^2 + \delta^2]^{-1/2} \\ h_{i,j}^{y\pm} &= \{1+\beta[(D_x^{0} f_{i,j})^2 + (D_y^{\pm} f_{i,j})^2]\}^{-1} \\ &\quad [(D_x^{0} u_{i,j}^n)^2 + (D_y^{\pm} u_{i,j}^n)^2 + \delta^2]^{-1/2} \\ \alpha_{i,j} &= \frac{\Delta t}{2} \left(h_{i,j}^{x+} + h_{i,j}^{x-} + h_{i,j}^{y+} + h_{i,j}^{y-} \right) \\ &\quad + \frac{\lambda_{i,j} \Delta t}{2\sqrt{(u_{i,j}^n - f_{i,j})^2 + \epsilon^2}} \,. \end{aligned}$$

   where $D_x^{\pm}$, D_x^0, $D_y^{\pm}$ and D_y^0 are the standard forward, backward and central difference operators in the x- and y-directions respectively.

3. For $i = 1, 2, \cdots, n_x$ and $j = 1, 2, \cdots, n_y$, compute

$$\begin{aligned} v_{i,j}^{n+1} &= \frac{1}{(1+\alpha_{i,j})} [(1-\alpha_{i,j}) v_{i,j}^n + \Delta t (h_{i,j}^{x+} v_{i+1,j}^n \\ &\quad + h_{i,j}^{x-} v_{i-1,j}^{n+1} + h_{i,j}^{y+} v_{i,j+1}^n + h_{i,j}^{y-} v_{i,j-1}^{n+1}) \\ &\quad + \frac{\Delta t \lambda_{i,j} f_{i,j}}{\sqrt{(v_{i,j}^n - f)^2 + \epsilon^2}}] \end{aligned} \qquad (32)$$

4. For $i = n_x, n_x - 1, \cdots, 1$ and $j = n_y, n_y - 1, \cdots, 1$, compute

$$\begin{aligned} w_{i,j}^{n+1} &= \frac{1}{(1+\alpha_{i,j})} [(1-\alpha_{i,j}) w_{i,j}^n + \Delta t (h_{i,j}^{x+} w_{i+1,j}^{n+1} \\ &\quad + h_{i,j}^{x-} w_{i-1,j}^{n} + h_{i,j}^{y+} w_{i,j+1}^{n+1} + h_{i,j}^{y-} w_{i,j-1}^{n}) \\ &\quad + \frac{\Delta t \lambda_{i,j} f_{i,j}}{\sqrt{(w_{i,j}^n - f)^2 + \epsilon^2}}] \end{aligned} \qquad (33)$$

5. Compute

$$u_{i,j}^{n+1} = \frac{1}{2} \left(v_{i,j}^{n+1} + w_{i,j}^{n+1} \right) \,. \qquad (34)$$

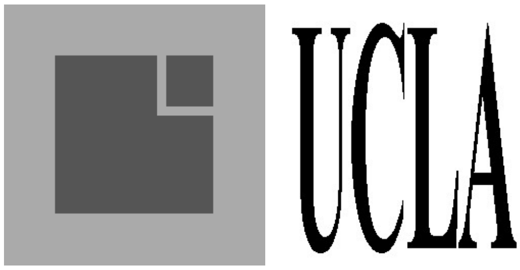

Figure 3. The original true image and the user defined mask.

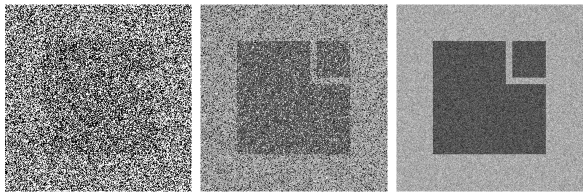

Figure 4. The original image with 75% salt-and-pepper noise, 50% random-valued impulse noise and additive Gaussian noise ($\sigma = 20$) respectively.

5 Examples

In the following examples, we use $u^0(x, y) = 0$ as the initial condition for the Euler-Lagrange equation. Unlike the classical active contour/snake model, different initial guesses used here will give the same **global** minimizer of the segmentation model in the case of binary images.

As discussed before, the ADE scheme has no stability condition imposed on Δt, and therefore we used $\Delta t = 100$ in all of the examples below.

5.1 Example 1

The true image used in this example has 256×256 pixels and is shown on the left in Figure 3. The user predefined mask is shown on the right. The dark region is the domain Ω' where we want to perform TV-inpainting. Figure 4 shows the noisy versions of the true image.

Figure 5 shows the denoised together with the segmented results of the image with 75% salt-and-pepper noise. The graphs show the intensity contour of the minimizer u. The salt-and-pepper noise is completely removed from the image. The red curves on the graph are the boundaries of the segmented regions. Unlike the minimization of the active contour model, we can now easily reach the global mini-

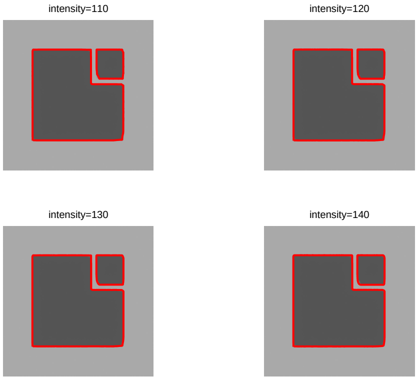

Figure 5. (Salt-and-Pepper) The minimizer for the energy (12) without an extra mask.

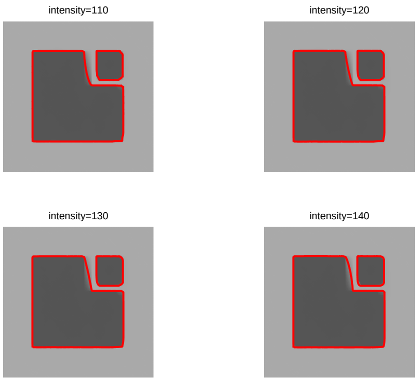

Figure 6. (Salt-and-Pepper) The minimizer for the energy (12) with an extra mask.

mum of the energy for this binary image regardless of the initial condition of the Euler-Lagrange equation. In the case of denoising together with image inpainting, the segmented results are shown in Figure 6. Again, the salt-and-pepper noise is removed completely from the image and we are able to fill in the missing part of the image using only one energy function. Figure 7 and 8 show the denoised, inpainted and segmented results when the random-valued impulse noise is added to the original true image. Figure 9 and 10 show the case when the additive Gaussian noise is added to the true image.

5.2 Example 2

The true image of Elaine used in this example has 512×512 pixels and is shown on the left of Figure 11. On the right, we give the predefined mask. 75% salt-and-pepper noise and 50% random-valued impulse noise are added to

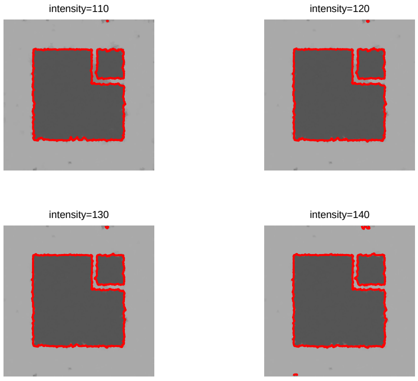

Figure 7. (Random-valued Impulse) The minimizer for the energy (12) without an extra mask.

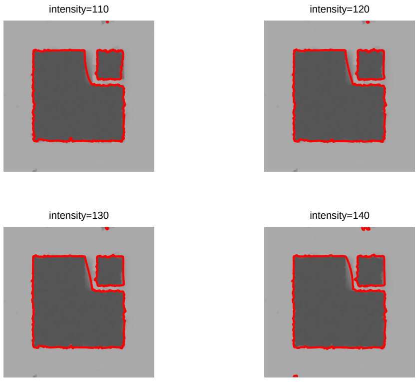

Figure 8. (Random-valued Impulse) The minimizer for the energy (12) with an extra mask.

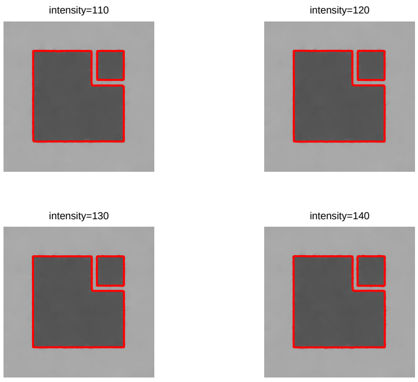

Figure 9. (Additive Gaussian) The minimizer for the energy (12) without an extra mask.

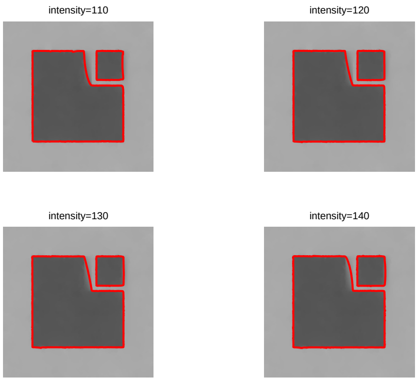

Figure 10. (Additive Gaussian) The minimizer for the energy (12) with an extra mask.

Figure 11. The original true image and the user defined mask.

Figure 12. The original image with 75% salt-and-pepper noise, 50% random-valued impulse noise and additive Gaussian noise ($\sigma = 20$) respectively.

Figure 13. (Salt-and-Pepper) The minimizer for the energy (12) without (left) and with (right) an extra mask.

Figure 14. (Random-valued impulse) The minimizer for the energy (12) without (left) and with (right) an extra mask.

Figure 15. (Additive Gaussian) The minimizer for the energy (12) without (left) and with (right) an extra mask.

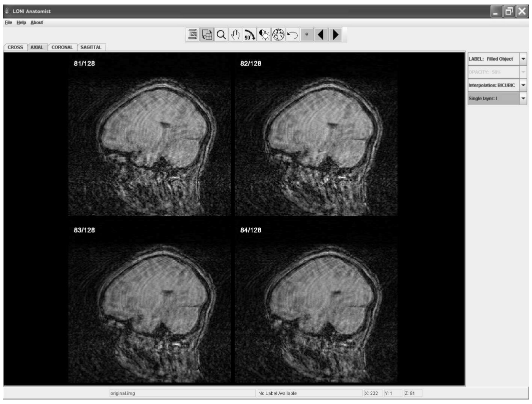

Figure 16. Some noisy brain MRI images.

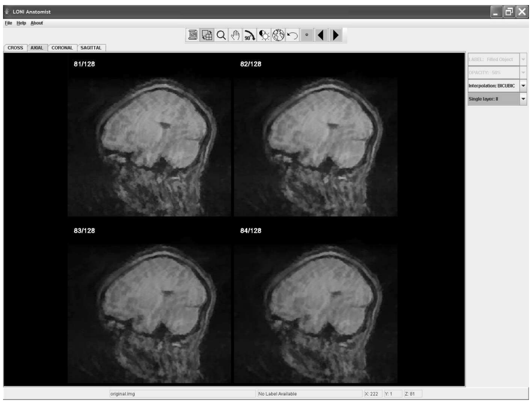

Figure 17. The corresponding denoised MRI images.

the original image and these observed images are shown on the left and middle of Figure 12, respectively. On the right hand side, we show the image with additive Gaussian noise with standard deviation $\sigma = 20$.

The minimizers of the energy functional (12) for these noisy images are shown in Figure 13 to 15. Figure 13 shows the results for the salt-and-pepper noise without (left) and with (right) an user defined mask function. Results for the random-valued impulse noise and the additive Gaussian noise are given in Figure 14 and 15.

5.3 Example 3

Figures 16 and 17 show the denoising results of a 3D brain MRI image. The number of voxels are $128 \times 256 \times 256$. The computational time is approximately 354 mins.

Acknowledgment

This work was supported in part by NSF contract DMS-0312222 and NIH contract U54 RR021813.

References

[1] X. Bresson, S. Esedoḡlu, P. Vandergheynst, J.P. Thiran, and S. Osher. Global minimizers of the active contour/snake model. *UCLA CAM Report (05-04)*, 2005.

[2] V. Caselles, R. Kimmel, and G. Sapiro. Geodesic active contours. *International Journal of Computer Vision*, 22(1):61–79, 1997.

[3] R. Chan, C.-W. Ho, and M. Nikolova. Salt-and-pepper noise removal by median-type noise detectors and detail-preserving regularization. *In preparation*, 2004.

[4] R. Chan, C. Hu, and M. Nikolova. An iterative procedure for removing random-valued impuse noise. *In preparation*, 2004.

[5] T.F. Chan, S. Esedoḡlu, and M. Nikolova. Algorithms for finding global minimizers of image segmentation and denoising models. *UCLA CAM Report (04-54)*, 2004.

[6] T.F. Chan and S.H. Kang. Error analysis for image inpainting. *UCLA CAM Report (04-72)*, 2004.

[7] T.F. Chan and J. Shen. Mathematical models of local non-texture inpainting. *SIAM J. Appl. Math.*, 62:1019–1043, 2001.

[8] S. Esedoḡlu and J. Shen. Digital inpainting based on the Mumford-Shah-Euler image model. *European Journal of Applied Mathematics*, 13:353–370, 2002.

[9] M. Kass, A. Witkin, and D. Terzopoulos. Snakes: Active contour models. *International Journal of Computer Vision*, 1(4):321–331, 1996.

[10] S. Kichenassamy, A. Kumar, P. Olver, A. Tannenbaum, and A.J. Yezzi. Conformal curvature flows: From phase transitions to active vision. *Archive for Rational Mechanics and Analysis*, 134:275–301, 1996.

[11] D. Mumford and J. Shah. Optimal approximation by piecewise smooth functions and associated variational problems. *Comm. Pure Appl. Math.*, 42:577–685, 1998.

[12] L. Rudin, S.J. Osher, and E. Fatemi. Nonlinear total variation based noise removal algorithms. *Physica D*, 60:259–268, 1992.